A Test of Bell's Inequality for the Undergraduate Laboratory

by

Burton A. Betchart

A thesis submitted in partial fulfilment of the requirements for

Honors

in the

Department of Physics and Astronomy

Oberlin College

May 2004

Abstract

The thesis documents the work done over the year to initiate an undergraduate Advanced Laboratory experiment which tests Bell's inequality. It provides reference theory for the experiment, including explanations of Bell inequalities, basics of nonlinear optics, type-I downconversion and entanglement, and polarization states of the entangled photons. A main result is the equipment and design proposal for the experiment, which will cost a total \$19600, led in price by the \$9000 of a four photodetector array and followed by the \$5000 of a $405nm$ pump laser. Entangled photons are produced by pumping BBO in a two-crystal geometry. Although most of the light is transmitted, some undergoes type-I parametric downconversion. Degenerate pairs are in a tunable entangled state and can be used to show non-classical behaviour. Specifically, a violation of the CHSH Bell inequality can be observed. Usable coincidence rates of several thousand per second are expected. Experimental and data analysis methods are described as the basis of future laboratory documentation. Explanations of equipment alignment and adjustment and data collection are included, as well as derivations of relevant analyses of the experimental data. Lastly the coincidence circuit built for the experiment is reviewed. The circuit costs less than \$40 to construct and demonstrates a coincidence window of between $18ns$ and $36ns$.

Table of Contents

List of Figures

List of Tables

Chapter 1: Introduction

The demonstration of the alocality of nature via a Bell inequality violation is an appealing experiment because it inspires a sense of wonder about the inner workings of the universe. Such an experiment is of interest not only for its inspirational value, but also for the wide range of physical topics it incorporates, including quantum mechanics, optics, electronics, and information theory. This thesis documents the work done over the year to initiate a Bell's inequality experiment in the undergraduate physics laboratory at Oberlin College. It includes introductory material, relevant theory, the experiment proposal, discussion of experimental methods and analysis, and a review of the coincidence electronics built this year.

1.1 History

Any history of the Bell inequalities begins with a paper published by Einstein, Podalsky, and Rosen (EPR) in 1935[1]. It is well known from Einstein's frequently quoted denial, "God does not play dice with the universe," that he had trouble accepting a quantum mechanical description of nature. The EPR paper was intended to be a positive step towards showing the existence of a more objective reality beyond the statistical superpositions described by quantum mechanics. It assumed the principle of *locality*, the notion that a measurement is only affected by quantities in the immediate vicinity, to show an apparent paradox in quantum mechanical descriptions of some two particle systems (entangled ones). They claimed that the paradox could be explained by the existence of some physical quantity which quantum mechanics misses completely, a so-called hidden variable.

In 1964, J.S. Bell published a theorem in the form of an inequality which holds for all local hidden variable theories, and is incompatible with quantum mechanical predictions[2]. In tests of the inequality, it is the principle of locality that stands to fail rather than quantum mechanics. Indeed, tests of Bell's inequality have shown violations of the conditions to which all local hidden variable theories must adhere.

The first tests of Bell's inequality were performed by Aspect, Grangier, and Roger in 1981[3, 4]. The group measured polarization correlations of photons emitted through the radiative atomic cascade of calcium and showed inequality violations. In the past ten years, Kwiat et. al. have developed better and brighter sources of polarization entangled photons based on the nonlinear optical process of spontaneous parametric downconversion[5, 6]. These sources are a main factor in enabling undergraduate institutions to develop Bell inequality experiments. Much of the work presented in this thesis was based on publications from several undergraduate institutions[7, 8, 9, 10].

1.2 Applications

There are many interesting applications of the nonlocal behaviour of entangled particles. Quantum cryptography utilizes the correlations of entangled particles to distribute cryptographic keys. Keys can be distributed securely over insecure channels with no previous secret because Bell-like inequalities prevent an unnoticed third-party observer[11, 12, 13]. Other related applications include the production of qubits for quantum computing[14]. Quantum computers can potentially run faster than any digital computer. Hard problems for digital computers such as the factoring of large numbers are the basis of modern cryptographic schemes. A quantum computer can accomplish this factoring in polynomial time[15]. It is interesting that the new quantum technology offers a new and more secure means of cryptography even as it threatens to break the current standard.

1.3 Outline

Chapter 2 provides the theoretical background necessary to the topics of this thesis. Section 2.1 discusses Bell inequalities and derives the CHSH inequality tested in the proposed experiment. Section 2.2 covers some basics of nonlinear optics relevant to the understanding of entangled photon production via spontaneous parametric downconversion. Section 2.3 derives some probability expressions for the entangled state used in the experiment.

Chapter 3 is a proposal for an Advanced Laboratory experiment to test Bell's inequality. The proposal describes the experiment and settles the major dilemmas over which equipment to purchase. It briefly mentions additional experiments which can be performed with the same equipment. The experimental methods themselves are documented in Chapter 4, and Chapter 5 treats the analysis of the data. Chapter 6 reviews the coincidence detecting electronics built for the experiment.

Chapter 2: Theory

This chapter treats the theory related to main topics of this thesis. Section 2.1 deals with Bell inequalities. Section 2.2 explains explains basic non-linear optics and a source of entangled photons produced by type-I parametric downconversion. Section 2.3 derives the quantum expression for the polarization states of of the downconverted photons.

2.1 Bell Inequalities

Quantum mechanics predicts phenomena which are counterintuitive to a classical understanding of nature, so much so that respected physicists have called into question how well the model represents actual physical reality[1]. Bell inequalities provide a means to test some of the most counterintuitive predictions of quantum mechanics. In order to understand how Bell inequalities work it is important to understand the concepts of completeness, locality, and entanglement[1, 16, 17].

Intuition from experience might lead us to expect that physical systems have definite objective properties. However any quantum mechanical model of a system cannot simultaneously describe definite values for all its physical properties, but instead describes a weighted superposition of states. As a matter of philosophy, one might choose to believe that all properties of natural systems always have definite objective values, and thus that the theory of quantum mechanics is *incomplete* in its inability to describe them. These definite values could be described if we had knowledge of some as yet unknown, or hidden, variables. This is the *realist* interpretation of quantum mechanics. Another option is to believe that quantum mechanics is a *complete* theory, that there are no hidden variables, and that physical reality is probabilistic rather than deterministic. This is the *orthodox* interpretation.

Based on intuition from both classical mechanics and special relativity we might expect physical reality to be *local*, which means that the result of any measurement depends only on the values of physical properties in the immediate space-time vicinity of the measurement. If the outcomes of measurements in two distinct space-time locations can be interdependent, then nature is *alocal* or *non-local*.

Two systems are called *entangled* if they are distinct, if they each exhibit superposition of states in some property q, and if knowledge of q for one particle implies knowledge of q for the other particle. As an example of entangled particles, consider a neutral pi meson that decays into a positron and an electron, which fly apart[18]. The pion has spin 0 and the positron and electron each have a spin of magnitude $\frac{1}{2}$. By conservation of angular momentum, measurement of the z-components of the positron's and electron's spin will be opposite. The orthodox interpretation of quantum mechanics is that neither particle has a definite z-component of spin be-

fore measurement, each being in a superposition of spin states. However, when one is measured and its z-component of spin is learned, the z-component of the other immediately assumes a definite direction. This interpretation clearly violates locality because the two particles can move arbitrarily far apart before measurement. If one adopts the realist position, then clearly the particles have definite z-components of spin from the moment they come into existence at the same point in space-time, and entanglement does not contradict locality.

In 1964, J.S. Bell published a theorem[1] which shows that *any* local hidden variable theory is incompatible with quantum mechanics[2]. Moreover, the disagreements between the two models can be tested experimentally. Results from such experiments closely follow quantum mechanical predictions and violate the Bell inequalities. This shows that nature cannot be local, regardless of whether the realist or orthodox interpretation is more accurate.

2.1.1   A Simple Example

The following example illustrates the nature of Bell inequalities and is derived from a *Physics Today* article by D. Mermin[17]. Consider a particle with a slippery shape property that is either square or round, depending on which way you look at it. The particle cannot be seen from two directions at once, and looking at it changes how it might have looked from other directions. A source creates entangled pairs of these particles, so that if you look at the two from the same angle they have the same shape, and sends them in opposite directions. Shape detectors independent of each other and of the source are placed in the path of each particle and randomly change between three observing angles after the particles are emitted. Because the particles are entangled, the detectors report the same shape every time they happen to measure a pair from the same observation angle. Additionally we find that the detectors measure the same shape for half of all runs when they are set arbitrarily and independently to one of the three angles. This last property does hold for some real systems, and is the key Bell found to show the existence of alocality.

In an effort to construct a model for this situation which is local in nature, we must assume that the information for shape appearance at each angle is carried on the particles. This is the only local way to ensure that the same shape is measured every time the detector angles happen to be the same. We can represent this information by either an s (for square) or r (for round) in three slots corresponding to the three detector angles. Remember that the shape is slippery; we can only observe the shape from one angle at a time, and subsequent measurement will not reflect what the shape "would have been" from another angle. Thus we can learn only two of the three pieces of information by measurement, one from each particle. The third number in each particle's instruction set is an unknowable, hidden variable.

Suppose a pair of entangled particles which look square from angles 1 and 2 and round from angle 3 each carry the instruction set ssr. For this particular instruction

---

[1] David Griffiths provides a clear explanation of Bell's Theorem[16]. For more information on Bell inequalities and hidden variable theories see [19].

set, there are five possible detector settings which yield the same shape (11, 22, 33, 12, 21) and four settings which yield different shapes (13, 23, 32, 31), so the probability of detecting the same shape given this instruction set is 5/9. There are five more possible instruction sets that also give probability 5/9 for detecting the same shape. These are RSS, SRS, RRS, RSR, and SRR. The only other possible instruction sets are RRR and SSS, for which the same shape is measured with probability 1. Whatever the distribution of these instruction sets among the entangled pairs, the detectors will measure the same shape in at least 5/9 of all runs.

The inequality $P \geq 5/9$, where P is the proportion over all runs that the detectors measure the same shape, is a Bell inequality for this particular local hidden variable model. However, one of the required features of any model is that it allow the observed behavior, that the same shape is observed in only half of all runs. Our inequality is violated; $P = \frac{1}{2} \ngeq \frac{5}{9}$, so our local hidden variable model does not adequately describe the system.

It is worth noting that this system can be created physically with spin-entangled electron/positron pairs substituted for the shape-entangled particles, and Stern-Gerlach analyzers substituted for shape detectors. The proper three angles to give $P = \frac{1}{2}$ are 0°, 120°, and 240°. The analog for a polarization entangled photon system is polarization detectors at angles 0°, 60°, and 120°, but because the linear polarizers only pass the vertical polarization of its rotated basis, measurements must be taken at the orthogonal angles as well. A better inequality for the polarization entangled system is presented in the next section. The angles for which quantum mechanics predicts violations of this inequality will be different.

2.1.2   The CHSH Bell Inequality

A Bell inequality published[20] in 1969 by Clauser, Horne, Shimony, and Holt is well suited to the experiment presented in this thesis[8]. It is derived again here for convenience.

Any local realistic interpretation of entanglement depends on a hidden variable λ, which could be a single variable or a set of variables. The values of λ affect the measurements of the entangled particles and vary according to unknown rules, but are distributed according to a probability $\rho(\lambda)$, where

$$\rho(\lambda) \geq 0, \tag{2.1}$$

and

$$\int \rho(\lambda)d\lambda = 1. \tag{2.2}$$

Suppose two particles are entangled in the property q and that measurement of q yields $+1$ or -1. In order for a theory describing this situation to be local, measurements of a particle at detector $\mathcal{A}$ must be completely determined by $\mathcal{A}$'s settings α and the local hidden variable λ. It is assumed that α can be set independently of λ. The result of a measurement at $\mathcal{A}$ is then given by some function $A(\lambda, \alpha) = \pm 1$.

Similarly, measurements at detector $\mathcal{B}$ are determined by $\mathcal{B}$'s settings β and a function $B(\lambda, \beta) = \pm 1$. The functions ρ, A and B can be any functions satisfying Eq. 2.1, 2.2, and $A, B = \pm 1$.

We can construct an inequality by the following arguments. The probability that $A = x$, where $x = \pm 1$, is

$$\langle A = x \rangle = \int \frac{1 + xA(\lambda, \alpha)}{2} \rho(\lambda) d\lambda.$$

Similarly, the probability that $A = x$ and $B = y$, for $x, y = \pm 1$, is

$$P_{xy}(\alpha, \beta) = \langle A = x, B = y \rangle = \int \frac{1 + xA(\lambda, \alpha)}{2} \frac{1 + yB(\lambda, \beta)}{2} \rho(\lambda) d\lambda. \tag{2.3}$$

We can define E,

$$E(\alpha, \beta) \equiv P_{++} + P_{--} - P_{-+} - P_{+-}, \tag{2.4}$$

as a a measure of particle correlation. E can take on values ranging from -1, when the detectors always disagree, to $+1$, when they always agree. It is easy to see from plugging in Eq. 2.3 that E is the expectation value of the product AB,

$$E(\alpha, \beta) = \int A(\lambda, \alpha) B(\lambda, \alpha) \rho(\lambda) d\lambda. \tag{2.5}$$

Next we define s,

$$
\begin{aligned}
s &\equiv A(\lambda, a) B(\lambda, b) - A(\lambda, a) B(\lambda, b') + A(\lambda, a') B(\lambda, b) + A(\lambda, a') B(\lambda, b') & (2.6) \\
&= A(\lambda, a)[B(\lambda, b) - B(\lambda, b')] + A(\lambda, a')[B(\lambda, b) + B(\lambda, b')], & (2.7)
\end{aligned}
$$

where a, a', b, b' are four distinct detector settings. Note that s can take on only the values ± 2. Now let S be the expectation value of s,

$$
\begin{aligned}
S(a, a', b, b') &= \langle s \rangle & (2.8) \\
&= \int s(\lambda, a, a', b, b') \rho(\lambda) d\lambda & (2.9) \\
&= E(a, b) - E(a, b') + E(a', b) + E(a', b'). & (2.10)
\end{aligned}
$$

Because s can only take on the values ± 2, $|S = \langle s \rangle| \leq 2$. This is a Bell inequality which quantum mechanics predicts will be violated in some situations, as will be shown in 2.3.

2.1.3   Loopholes

To date, the experiments to test Bell inequalities have all had loopholes, although most of them are far-fetched. For example, one can create a local realistic scenario if the distribution of λ were affected by the choice of detector settings α and β before the entangled particles where created. To close this loophole, the settings need to be chosen after the particles are "in flight". This particular scenario is called the "rapid switching loophole". For more information on loopholes and suggested loophole-free experiments, see [21, 22].

2.2 Entangled Photon Production

Polarization entangled photons were first produced in the 1980s using a process called radiative atomic cascade, in which a change from one zero angular momentum state to another causes two photons to be emitted from a calcium atom[3, 4, 23]. Although this source provided adequate photons for a Bell's inequality experiment, it suffered timing and inefficiency problems due to recoil of the parent atom between photon emissions. A better source allowing maximally entangled forms of all four Bell states was realized in 1995 using a parametric downconversion process with type-II phase matching[5]. In 1998 a group used spontaneous parametric downconversion with a two-crystal geometry and type-I phase matching to produce the brightest source yet of entangled photons[6]. This last source allows the same flexibility in entanglement state as the previous one. This section explains the two-crystal geometry downconversion source, as well as necessary background theory.

2.2.1 Non-linear Optics

The polarization of most materials responds linearly to an applied electric field according to its linear susceptibility $\chi^{(1)}$. Non-linear materials have significant higher order terms in the power series expansion for the polarization. Discussion in this paper [24] is limited to the quadratic term,

$$\left| \mathbf{P^{(2)}} \right| = \epsilon_0 \chi^{(2)} \left| \mathbf{E} \right|^2 . \tag{2.11}$$

In general, $\chi^{(2)}$ is directionally dependent, and is written as a tensor so that

$$P_i^{(2)} = 2\epsilon_0 \sum_{jk} \chi_{ijk}^{(2)} E_j E_k. \tag{2.12}$$

The susceptibility is commonly represented by d-coefficients, with the d tensor given by

$$d_{ijk} = \frac{1}{2} \chi_{ijk}^{(2)}.$$

Due to the symmetry of most materials, the d tensor is usually written in contracted form d_{lm}, where $l = (1, 2, 3)$ correspond to $i = (x, y, z)$ and $m = (1, \ldots, 6)$ represent two directions according to $jk = xx \rightarrow m = 1$, $yy \rightarrow 2$, $zz \rightarrow 3$, $yz = zy \rightarrow 4$, $xz = zx \rightarrow 5$, and $xy = yx \rightarrow 6$.

In many non-linear optical materials the index of refraction depends on the direction of the electric field vector. Birefringent materials can be characterized by two indices of refraction, one for ordinary rays and one for purely extraordinary rays. The *optic axis* of a birefringent material is the direction along which a ray of any polarization will travel at the same speed. An ordinary ray has polarization orthogonal to the optic axis, while a purely extraordinary ray has polarization parallel with optic axis, as shown in Fig. 2.1(a). The ordinary ray is subject to the ordinary index of refraction, n_o, while $\bar{n}_e$ is the index of refraction for the extraordinary ray. Rays with polarization
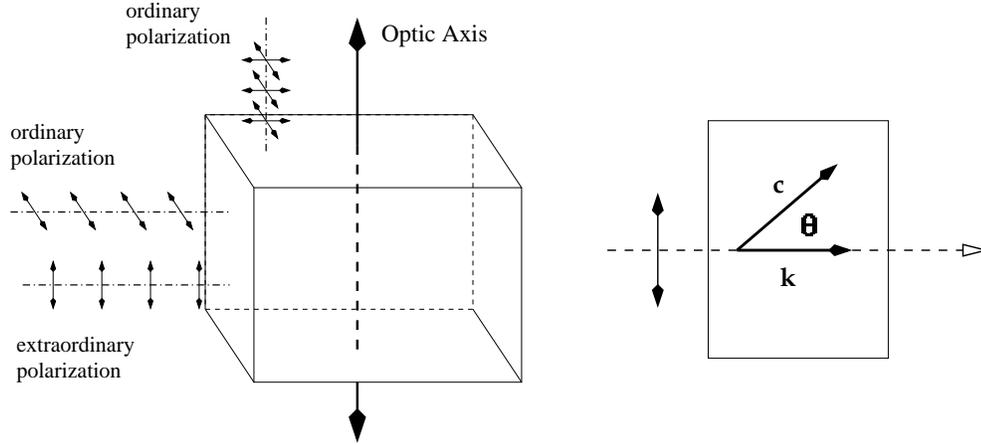
(a) Diagram of a birefringent material showing the relative geometry of ordinary and extraordinary rays with the optical axis.

(b) A wave polarized in the plane defined by the optic axis **c** and its propagation vector **k** has an effective index of refraction related to n_o, $\bar{n}_e$, and θ. See Eq. 2.13

Figure 2.1: The optical geometry of birefringence.

in the plane of the optic axis propagate according to an effective index of refraction n_e given by the relation

$$\frac{1}{n_e(\theta)^2} = \frac{\sin^2\theta}{\bar{n}_e^2} + \frac{\cos^2\theta}{n_o^2},\qquad(2.13)$$

where θ is the angle between the optic axis and propagation direction, as shown in Fig. 2.1(b). In general materials are dispersive, and $\bar{n}_e = \bar{n}_e(\lambda)$ and $n_o = n_o(\lambda)$, where λ is the wavelength, are given by the Sellmeier equations. Birefringent materials are called *negative* or *positive* according to the sign of $\bar{n}_e - n_o$.

2.2.2   Optical Parametric Processes.

In optics, parametric processes are those for which energy and momentum are conserved for three photons interacting in a non-linear medium. These processes include second harmonic generation (SHG, $\omega_{SHG} = \omega_P + \omega_P$), sum frequency generation (SFG, $\omega_S = \omega_{P1} + \omega_{P2}$), and difference frequency generation (DFG, $\omega_D = \omega_{P1} - \omega_{P2}$). The coupled equations for optical parametric processes can be generally written as three first order partial differential equations[24, 25].

SHG is the easiest of these examples to understand. A simplified model of the electric field of a linearly polarized laser beam is

$$E^{(\sim)} = E_0 \cos[kx - \omega t],$$

where k is the angular wave number and ω is the angular frequency. The second

order term of the polarization for a particular point in the non-linear medium is then

$$P \propto \cos^2[\omega t] = \frac{1}{2} + \frac{1}{2}\cos[2\omega t],$$

so the quadratic term of the polarization can be thought of as creating a constant DC polarization and transmitted radiation with double the pump frequency. However, the second harmonic cannot propagate in arbitrary directions through the medium. Momentum conservation requires that $\mathbf{k}_{(2\omega)} = 2\mathbf{k}_\omega$. Because $|\mathbf{k}| = \frac{\omega n}{c}$, we can rewrite this expression as $n_{2\omega} = n_\omega$. In other words, SHG requires that light with the second harmonic frequency propagate at the same speed as light with the pump frequency. Some materials can satisfy this relation for specific conditions.

In general, momentum conservation is equivalent to requiring that the generated beam's component parallel to the pump beam propagate in phase with the pump beam. This makes sense, because otherwise photons generated at different points along the path of the pump beam would interfere destructively. Finding the appropriate conditions for a particular parametric process is called phase matching. Dispersion relations, birefringence, and temperature dependence of refractive indices allow phase matching to be achieved by choosing appropriate frequencies, angles, and temperatures.

Spontaneous parametric downconversion (SPDC), also known as optical parametric oscillation or optical parametric fluorescence, is described by the energy conservation $\omega_p = \omega_s + \omega_i$ and momentum conservation $\mathbf{k}_p = \mathbf{k}_s + \mathbf{k}_i$. The subscripts s and i stand for *signal* and *idler*, for historical reasons. SPDC can be thought of as the inverse of SFG[8, 25].

2.2.3 Type-I SPDC

Spontaneous parametric downconversion occurs when a pump photon interacting with a non-linear medium splits into signal and idler photons subject to the energy and momentum conservation conditions

$$\omega_s + \omega_i = \omega_p \tag{2.14}$$

and

$$\mathbf{k}_s + \mathbf{k}_i = \mathbf{k}_p, \tag{2.15}$$

where the subscripts s, i, and P correspond to the signal, idler, and pump photons, and ω and $\mathbf{k}$ are the angular frequency and wave vector. As shown in Fig. 2.2, type-I phase matching conditions produce signal and idler photons with the same polarization, opposite the pump polarization[2]. Only one polarization of the pump beam will trigger type-I downconversion, but the signal and idler pair produced can lie in any common plane with the pump beam. The collection of all signal and idler pairs, all polarized opposite the pump beam, form concentric cones around the pump beam with angles according to their energy split.

---

[2] Type-II phase matching conditions produce a signal and idler with opposite polarizations.
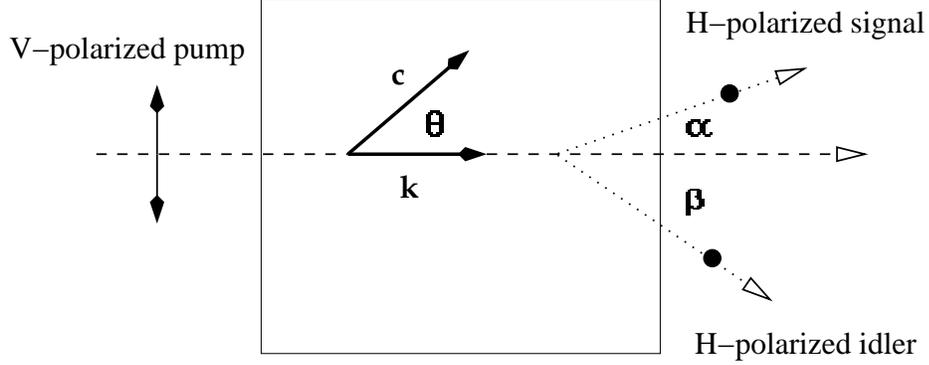
Figure 2.2: A pump photon splits into signal and idler photons in type-I phase matched SPDC.

To find the phase matching angles α and β for a signal/idler pair, first use $|\mathbf{k}| = \omega n/c$ and the approximation $n_o(\omega_s) \approx n_o(\frac{1}{2}\omega_p) \approx n_o(\omega_i)$ to rewrite Eq. 2.15 as

$$\omega_s \sin\alpha + \omega_i \sin\beta = 0$$

and

$$\omega_s \cos\alpha + \omega_i \cos\beta = \frac{\omega_p n_e(\omega_p, \theta)}{n_o(\frac{1}{2}\omega_p)}.$$

For the degenerate case $\omega_s = \omega_i = \frac{1}{2}\omega_p$, it is clear that $\alpha = -\beta$. Substituting into the rewritten form of 2.15 yields

$$\frac{1}{n_e(\omega_p, \theta)} = \frac{\sec\alpha}{n_o(\frac{1}{2}\omega_p)}.$$

Combining this result with Eq. 2.13 gives the relation between crystal cut, pump frequency, and phase matching angle

$$\frac{\sin^2\theta}{\bar{n}_e(\omega_p)^2} + \frac{\cos^2\theta}{n_o(\omega_p)^2} = \frac{\sec^2\alpha}{n_o(\frac{1}{2}\omega_p)^2}, \tag{2.16}$$

which can be solved explicitly given the indices of refraction.

2.2.4   BBO

Beta barium borate, also written $\beta\text{-}BaB_2O_4$ and BBO, is a common non-linear optical material. Its useful characteristics include transparency over a large bandwidth from UV through infrared, wide phase-matching capabilities, high damage threshold, and low hygroscopic susceptibility. Table 2.1 shows some properties of BBO. Fig. 2.3 graphs the Sellmeier equations for BBO's indices of refraction as a function of wavelength. Fig. 2.4 shows a graph of Eq. 2.16 solved for BBO.

17

Crystal Structure	Trigonal
Crystal Symmetry	3m
Transmission Range	$0.2 - 3\mu m$
Damage threshold	$5\ GW/cm^2$
Birefringence	negative uniaxial
NLO d-coefficients $\left(\frac{pm}{V}\right)$	

$$d_{11} = 2.3$$
$$d_{31} = 0.15$$
Type-I $d_{\text{eff}} = d_{31}\cos\theta$

Sellmeier equations (λ in μm)
$$n_e(\lambda)^2 = 2.7359 + \frac{0.01878}{\lambda^2 - 0.01822} - 0.01354\lambda^2$$

$$n_o(\lambda)^2 = 2.3753 + \frac{0.01224}{\lambda^2 - 0.01667} - 0.01515\lambda^2$$

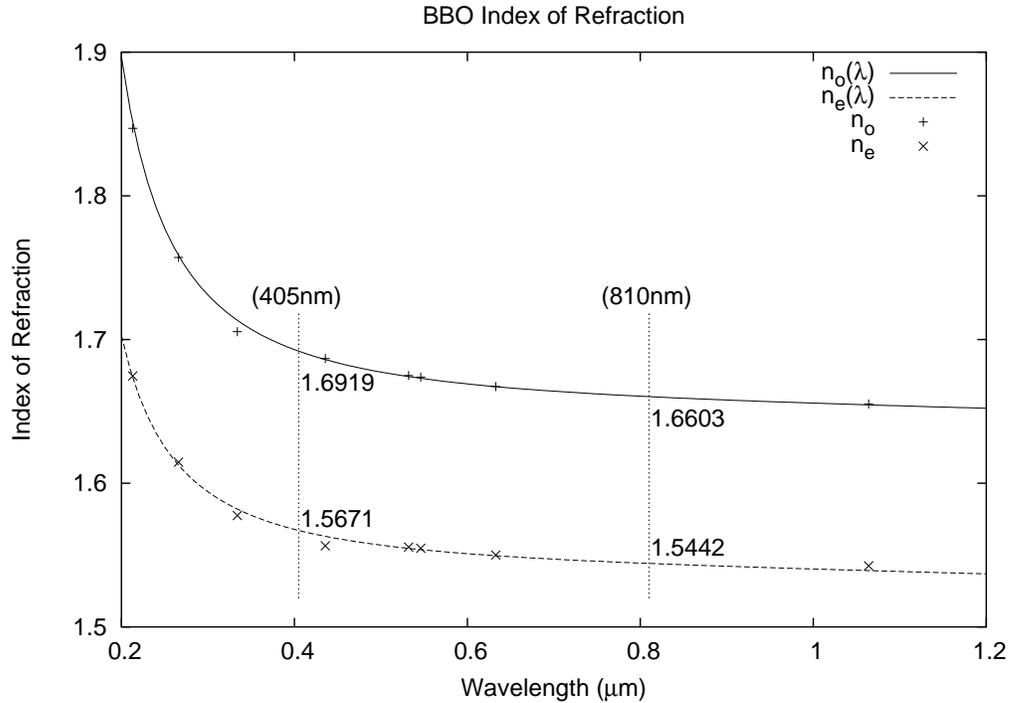**Table 2.1:** Properties of BBO[24, 26, 27, 28].

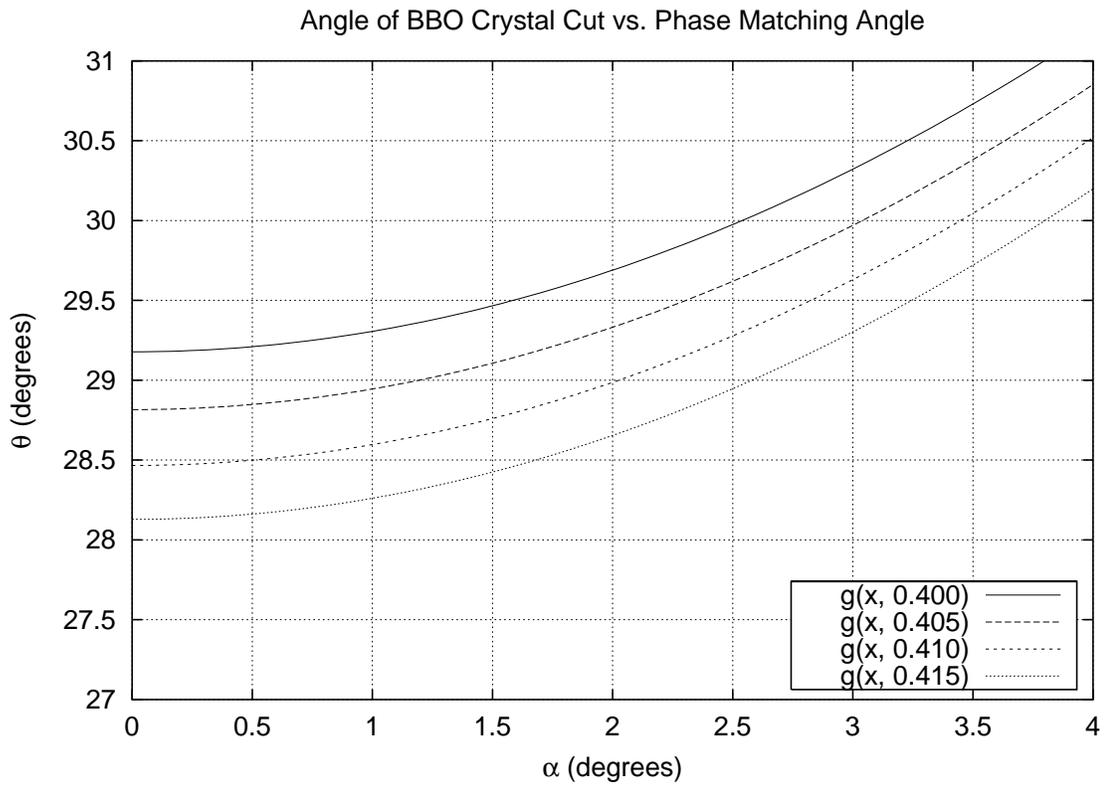**Figure 2.3:** The indices of refraction for BBO are given by the Sellmeier equations, shown in Table 2.1

Figure 2.4: BBO crystal cut as a function of the degenerate phase matching angle at pump wavelengths from $400nm$ to $415nm$. The downconversion efficiency is related to $\cos^2\theta$, so a 30° crystal cut is appropriate for a $405nm$ pump laser.
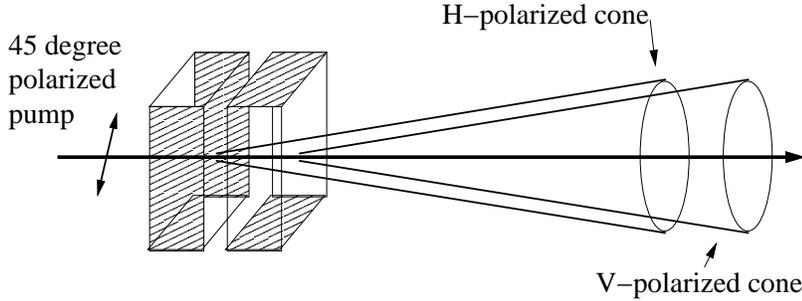
Figure 2.5: A two crystal downconversion source with appropriately thin crystals creates overlapping, and thus entangled, cones of downconverted light.

2.2.5 Entangled Photons

Photons in an entangled state can be produced with type-I phase matching SPDC by using a two crystal geometry[6, 8]. Specifically, entangled photons will be produced by two thin crystals identically cut for type-I phase matching and mounted orthogonally back to back. Vertically polarized light passing through this arrangement can downconvert in the first crystal, while horizontally polarized light can downconvert in the second. A 45° polarized pump photon is equally likely to downconvert in either crystal, neglecting losses of passing through the first. If the crystals are relatively thin, photons produced in the first crystal are not spatially or timing distinguishable from photons produced in the second. The photons are then in a superposition state of VV or HH, with superposition the last fulfilled of the properties required for entanglement (the pair have a definite property with just one crystal, but the polarization state is known). Conversely, if the crystals are too thick, the horizontal and vertical polarized cones will not overlap and the two states will be spatially labeled. Fig. 2.5 shows a diagram of the two crystal downconversion arrangement.

We can mathematically describe the operation of the two crystals as

$$|V\rangle_p \rightarrow |H\rangle_s |H\rangle_i$$

$$|H\rangle_p \rightarrow e^{i\Delta} |V\rangle_s |V\rangle_i \tag{2.17}$$

where Δ is a phase shift due to birefringence and dispersion of the crystals. A pump beam with polarization θ_p from the vertical and phase shift ϕ_p between vertically and horizontally polarized components is described by

$$|\psi_{pump}\rangle = \cos\theta_p |V\rangle_p + e^{i\phi_p} \sin\theta_p |H\rangle_p. \tag{2.18}$$

Merging 2.17 into 2.18 gives us

$$|\psi_{DC}\rangle = \cos\theta_p |H\rangle_s |H\rangle_i + e^{i\phi} \sin\theta_p |V\rangle_s |V\rangle_i, \tag{2.19}$$

where $\phi = \Delta + \phi_p$ is the total phase difference between horizontal and vertical polarization components. Signal and idler photon pairs described by $|\psi_{DC}\rangle$ are entangled in their polarizations.

Photons produced by the parametric process described are called "hyperentangled" because they are simultaneously entangled in all degrees of freedom[29]. However, it is conceptually and experimentally easiest to deal with the polarization entanglements described by 2.19. Two of four Bell states can be produced with this arrangement: $HH \pm VV$, when $\theta_p = \pi/4$ and $\phi_p = 0, \pi$. The two remaining Bell states $HV \pm VH$ can be created by inserting a half wave plate, which rotates polarization[34], in either the signal beam or the idler beam. Non-maximally entangled states of the form $HH + \epsilon VV$, $|\epsilon| \neq 1$, can be created by setting $\theta_p = \arctan \epsilon$, and can be useful in loophole-free tests of Bell's inequality[22].

2.3 Polarization States of Downconverted Photons

In Section 2.1.2 we posited a system of two particles entangled in a property q, and for which a measurement of q yields ± 1. We saw that for such a system, the inequality $|S| \leq 2$ holds for any local hidden variable theory. This section derives the quantum mechanical expression for S in a system of polarization entangled photons. The quantum mechanical model proposes no hidden variables, and predicts $S > 2$ for some situations.

Recall Eq. 2.4 and 2.10, that

$$E(\alpha, \beta) = P_{++} + P_{--} - P_{-+} - P_{+-},$$

$$S = E(a, b) - E(a, b') + E(a', b) + E(a', b'),$$

where α and β are settings for detectors $\mathcal{A}$ and $\mathcal{B}$, $P_{*\dagger}$ represents the probability that detector $\mathcal{A}$ measures state $*$ and detector $\mathcal{B}$ measures state $\dagger$, and a, a', b, b' are four distinct detector settings. For our two photon system, the entangled property q is the polarization, which is measured as either $|V\rangle$ or $|H\rangle$ corresponding to $+1$ and -1, respectively. The detector settings α and β are the angles of linear polarizers relative to the lab frame. If we can find an expression for $P_{VV}(\alpha, \beta)$, we can find

$$E(\alpha, \beta) = P_{VV}(\alpha, \beta) + P_{VV}(\alpha_\perp, \beta_\perp) - P_{VV}(\alpha_\perp, \beta) - P_{VV}(\alpha, \beta_\perp), \qquad (2.20)$$

assuming the distribution remains constant over time. With sixteen measurements of P_{VV} we can find $S(a, a', b, b')$.

A linear polarizer set to angle γ will transmit light it measures in state $|V_\gamma\rangle$ and block light it measures as $|H_\gamma\rangle$. In the $|V\rangle$, $|H\rangle$ basis, the states $|V_\gamma\rangle$ and $|H_\gamma\rangle$ are written as

$$|V_\gamma\rangle = \cos \gamma \, |V\rangle - \sin \gamma \, |H\rangle,$$

$$|H_\gamma\rangle = \sin \gamma \, |V\rangle + \cos \gamma \, |H\rangle. \qquad (2.21)$$

Due to noise, a photon detected behind a polarizer may not be from an entangled pair. However, the probability is small for two noise related photons to be detected simultaneously. The probability of detecting both the signal and idler photons behind linear polarizers set to angles α and β is

$$P_{VV}(\alpha, \beta) = \left| \langle V_\alpha|_s \langle V_\beta|_i \, |\psi_{DC}\rangle \right|^2, \qquad (2.22)$$

21

where $|\psi_{DC}\rangle$ is given by Eq. 2.19. We can substitute Eq. 2.21 into the expression for $P_{VV}(\alpha, \beta)$ and simplify with $\langle V||V\rangle = 1$, $\langle V||H\rangle = 0$, and $|\psi|^2 = \psi^*\psi$ as follows:

$$
\begin{aligned}
P_{VV}(\alpha, \beta) &= \left| \langle V_\alpha|_s (\cos\beta \langle V|_i - \sin\beta \langle H|_i)(\cos\theta |H\rangle_s |H\rangle_i + e^{i\phi}\sin\theta |V\rangle_s |V\rangle_i) \right|^2 \\
&= \left| (\cos\alpha \langle V|_s - \sin\alpha \langle H|_s)(\cos\beta \sin\theta |V\rangle_s e^{i\phi} - \sin\beta \cos\theta |H\rangle_s) \right|^2
\end{aligned}
$$

$$
= \left| \cos\alpha \cos\beta \sin\theta e^{i\phi} + \sin\alpha \sin\beta \cos\theta \right|^2 \tag{2.23}
$$

$$
\begin{aligned}
&= (\cos\alpha \cos\beta \sin\theta e^{-i\phi} + \sin\alpha \sin\beta \cos\theta)(\cos\alpha \cos\beta \sin\theta e^{i\phi} + \sin\alpha \sin\beta \cos\theta) \\
&= \cos^2\alpha \cos^2\beta \sin^2\theta + \sin^2\alpha \sin^2\beta \cos^2\theta \\
&\qquad\qquad + \sin\alpha \cos\alpha \sin\beta \cos\beta \sin\theta \cos\theta (e^{i\phi} + e^{-i\phi})
\end{aligned}
$$

$$
= \cos^2\alpha \cos^2\beta \sin^2\theta + \sin^2\alpha \sin^2\beta \cos^2\theta + \frac{1}{4}\sin 2\alpha \sin 2\beta \sin 2\theta \cos\phi \tag{2.24}
$$

Photon pairs collected over a finite solid angle and wavelength range will have a spread in the phase lag ϕ. The actual state collected is better represented by substituting $\langle\cos\phi\rangle = \cos\phi_m$ for $\cos\phi$.

Special cases occur when $\theta = \pi/4$ and $\phi = 0, \pi$. Then

$$
\left| \psi_{DC}^\pm \right\rangle = (|H\rangle_s |H\rangle_i \pm |V\rangle_s |V\rangle_i)/\sqrt{2}, \tag{2.25}
$$

and $P_{VV}(\alpha, \beta)$ simplifies from Eq. 2.23 to

$$
P_{VV}(\alpha, \beta) = \frac{1}{2}\cos^2(\alpha \mp \beta), \tag{2.26}
$$

which depends only on the relative angle $\alpha \mp \beta$. For a better understanding of how S varies with for different sets of four angles, the reader may wish to use these mathematically simple cases and plug in angles to find some values of S. For example, quantum mechanics predicts S has a maximum of $2\sqrt{2} > 2$ for the set of angles $(a, a', b, b') = (-\frac{\pi}{4}, 0, -\frac{\pi}{8}, \frac{\pi}{8})$, which violates the Bell inequality derived earlier.

Chapter 3: Proposal

Experiments in quantum optics with entangled photons have recently become feasible in undergraduate laboratories due to advances in non-linear optics and in laser diode and detector technologies. The newly attainable experiments include a test of Bell's inequality using entangled photon polarizations[2]. Kwiat et. al. pioneered new sources of entangled photons in the past 10 years and originally proposed that these sources might make undergraduate experiments possible[5, 6]. An experiment at Reed College realized this possibility[7, 8]. Similar experiments are being developed at Colgate University and Whitman College[9, 10].

This chapter presents an experiment to test Bell's inequality in the style of the experiments cited above, with thought given to both cost and extension to other experiments. The equipment of best value for this and future experiments will cost $19600 and fit on the department's optics table. Extensions to this apparatus in the future will allow experiments showing the existence of discrete photons, as in the 1986 Grangier experiment[23], the interference of a single photon with itself, and other quantum optics experiments[30]. These can be added successively for about $1000 each.

3.1   Description of Experiment

Fig. 3.1 shows the experiment to test Bell's inequality. Light from a pump laser passes through a non-linear crystal and undergoes spontaneous parametric downconversion into signal and idler photons. These photons are created in the same instant and have definite combined properties due to energy and momentum conservation[24]. Polarization entangled photons can be produced along certain directions via type-II downconversion[5] or type-I downconversion using a two crystal geometry[6].

Single photons are detected by Si Avalanche Photodiodes which output $25ns$ TTL pulses upon detection. A coincident photon detection event is most likely the result of two photons created at the same instant by downconversion. Photons detected in coincidence are deemed to be polarization entangled.

By measuring the rate of coincidences as a function of polarization filter angles, an experimenter can show violations of a Bell inequality. The CHSH Bell inequality derived in Section 2.1.2 shows that a quantity S derived from the coincidence rates is bound by the inequality $|S| \leq 2$ for any local hidden variable theory[20]. The quantum mechanical model, not bound to rules of locality, predicts $S > 2$ for some angles. Experiment confirms the quantum mechanical prediction.
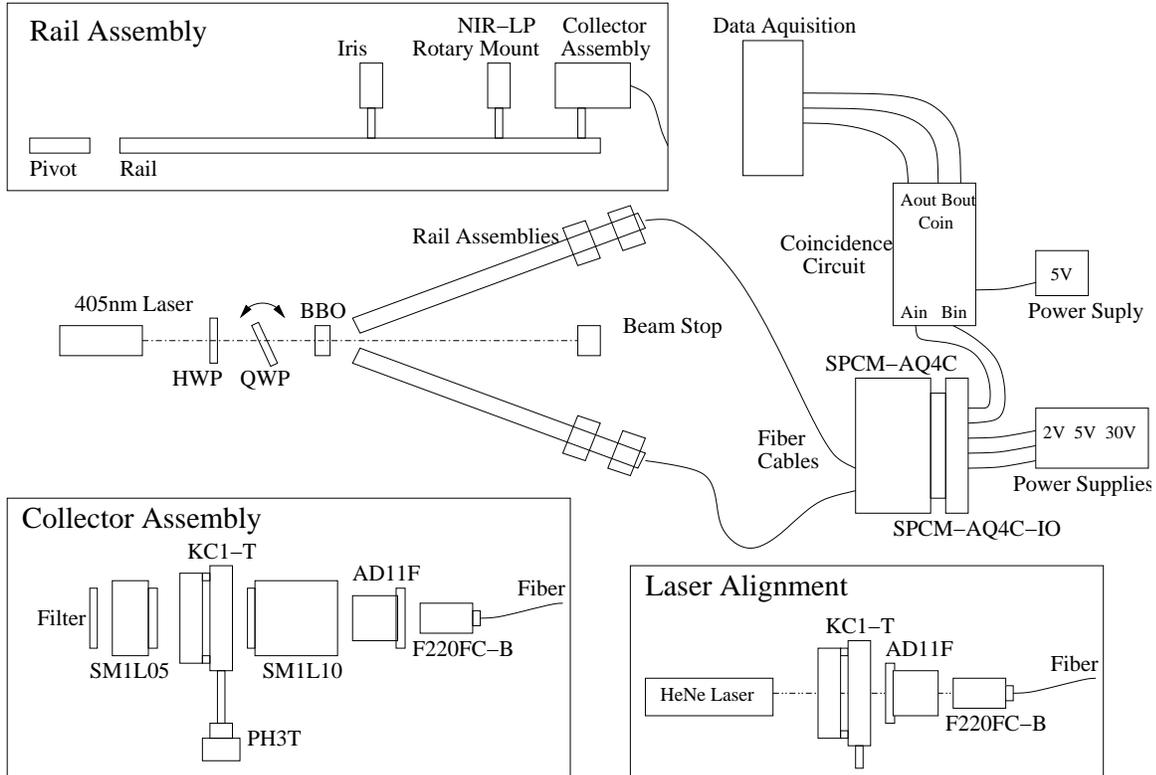
Figure 3.1: Light from a pump laser passes through a non-linear crystal (BBO) to produce polarization entangled photons. Photons collected within the coincidence window are assumed to be entangled. These photons can be used to show non-classical behaviour such as a violation of Bell's inequality.

3.2 *Equipment*

The equipment described in this section enables a test of a Bell inequality and provides a platform for additional experiments in quantum optics at a cost of $19600. Table 3.1 shows the equipment to be purchased with prices and suppliers. It does not include the following necessary equipment already owned by the department: optics table, computer, HeNe laser, coincidence circuit w/ $5VDC$ power supply, BNC cables. The most costly piece of equipment for this experiment is the avalanche photodiode array, at $9000. This array of 4 detectors, along with accompanying fiber optics, raises the cost of the system two to four thousand dollars over a system with 2 single non-fiber detectors. However, the cheaper route is more expensive to extend to experiments with 3 and 4 detectors and looses the advantages of fiber optics.

3.2.1 *Entangled Photon Production*

A two crystal geometry of β-barium borate (BBO) crystals cut for type-I downconversion will give the brightest source of entangled photons[6]. With the two crystals

mounted orthogonally, a 45° polarized pump photon is equally likely to downconvert in either crystal, producing the entangled state $HH + e^{i\phi}VV$, where ϕ is a phase difference due to crystal birefringence. A crystal cut of 30° between the normal face and the optic axis for both crystals is appropriate for 405-409nm pump wavelengths, as shown in Fig. 2.4. The crystals should be ordered in a mount with P-coating. These last two options provide a simpler solution than a crystal in a housing and will prevent the surface of the crystal from becoming fogged[28].

The proportion of downconverted photons is proportional to the square root of the intensity of the pump beam. The selected 20mW pre-polarized laser will produce about 5Ms^{-1} degenerate pairs on the full cone, or about 20ks^{-1} pairs incident on the detectors. Detector and polarizer inefficiencies will reduce this rate to about 3ks^{-1}.

A half wave plate (HWP) before the BBO in a rotary mount allows the control of pump polarization. The phase angle ϕ can be adjusted by tilting a quartz quarter wave plate (QWP) also before the BBO. This tunes the entanglement state of the downconverted photons. The QWP is mounted on a rotation stage for calculated tilting.

3.2.2 Photon Collection

Collection components are mounted on an optics rail which allows freedom of angular adjustment while maintaining alignment. The rails pivot about the downconversion crystal's mounting post. In addition to the collector assembly, each optics rail has an iris diaphragm and a rotary mounted near-IR linear polarizer. The iris limits the signal bandwidth because the downconversion output frequency is dependent on propagation direction. Polarizer settings affect coincidence rates in a way which shows a violation of a Bell inequality. The polarizers transmit 70% v-polarized, and 0.2% h-polarized light. They must be cut to size from a sheet.

The collector assembly provides coupling of the signal beam into a fiber optic cable and filters out light from non-signal bandwidths. The translating post holder and kinematic mount allow for adjustments of the fiber coupling lens. The filter's small passband of 10nm FWHM helps to protect the detectors against overload damage. The filter is easy to remove in order to allow alignment by shining a HeNe laser through the collector in reverse. Ordering of the filters should be postponed until after obtaining the pump laser. After measuring the lasers spectrum, filters centered at double the the peak wavelength can be ordered.

Optic connections between the collector↔detector and collector↔alignment laser must be completely opaque to outside light and are made via fiber cables with standard commercial FC type connectors. An FC to FC mating sleeve with L-bracket allows switching of fiber paths between collector and detector/alignment laser without disturbing the collector alignment or wearing on the detector connections.

The reverse laser alignment requires another fiber coupling lens and kinematic mount to align the HeNe laser into the fiber. The HeNe laser shining back through the collector should overlap the pump laser spot on the downconversion crystal.

		Part Number	Cost($)	Qt.	Comments
Entangled Photon Production					
Laser	●	NT55-872	5495	1	>20mW, beam diam <1.5mm, linearly polarized, 405±10nm, 1 year waranty, power supply included.
Half Wave Plate	✠	WPZ1310	142	1	400nm airspaced zero-order HWP in 1" mount
Quarter Wave Plate	✠	WPZ1310	142	1	400nm airspaced zero-order QWP in 1" mount
BBO	≀	Custom	1400	1	Two 30° cut BBO crystals 0.1x5x5mm, mounted 90°, with P-coating.
Rail Assembly					
Rail	∗	RLA2400	129	2	24x0.75x0.37" optics rail.
Pivot		Al bar	10	1	Build pivot from Al bar.
Iris	∗	ID12	38	2	0.8-12mm aperture, w TR3 mount.
NIR-Linear Polarizer	●	NT54-111	206	1	800-2000nm plastic film LP, 34% princ trans. 2x2"
Clamp	∗	CL5	4	2	Clamp for holding rail in place.
Collector Assembly					
Filter	‡	F10-810.0-4-0.50	80	2	0.5" 810nm bandpass filter, 10nm FWHM.
1/2" Lens Tube	∗	SM1L05	13	2	0.5" stackable lens tube, SM1.
1" Lens Tube	∗	SM1L10	15	2	1" stackable lens tube, SM1.
Fiber Coupler Adapter	∗	AD11F	26	3	SM1 adapter.
Fiber Coupler	∗	F220FC-B	132	3	0.25" aperture, FC connection, 600-1050nm.
Photon Detection					
Fiber Cables	∗	M31L01	48	5	1 meter, multimode, 62.5μm core, FC connectors.
FC to FC connector	∗	FCB1	44	1	FC to FC Dual Mating Sleeve L-Bracket.
Photon Detectors	◇	SPCM-AQ4C	9000	1	4 SiAPD array with FC inputs, 1 year waranty.
SPCM-AQ4 IO	◇	SPCM-AQ4C IO	265	1	Power, gate, and signal interface.
30V DC Power			100	1	DC 30V ±1.5V, typical 0.3W, max 1.2W.
5V DC Power	◇	SPCM Power Supply	66	1	DC 5V ±0.5V, typical 1W, max 5W.
2V DC Power			100	1	DC 2V ±0.1V, typical 2W, max 6W.

Data Aquisition					
PCI Counter/Timer	†	PCI-6601	295	1	4 ↑↓ 32-bit cntr/tmr, 20MHz source max.
Ribbon Cable	†	R6868	40	1	Low cost unsheilded, 1 meter.
IO Connector Block	†	CB-68LP	70	1	Low cost unsheilded, 68 pin.
Mounts					
Posts	∗	TR3	6	7	3", 0.499" diam steel post.
Bases	∗	BA1	6.5	3	Post base, 1x3x0.37".
Post Holders	∗	PH3-ST	9	8	Post holder with thumbscrew.
Translating Post Holders	∗	PH3T	48	2	translates height 2.19-2.63"
Kinematic Mounts	∗	KC1-T	84	3	5°, 3mm trans, lockable, SM1 compatable.
Rotary Mounts	∗	RSP1	76	3	2° increments, full range.
Rotation Stage	∗	RP01	83	1	Rotation stage for quarter wave plate.
QWP Holder	∗	CP02	16	1	SM1 threads, joins to TR3.
Miscellaneous					
Beam Stop	∗	LB1	41	1	0.75x1.5" active area, w TR3 mount.
Spanner Wrench	∗	SPW602	26	1	For optics assembly.
			$19600		**Total Cost**

Table 3.1: Purchases necessary for a Bell's Inequality Experiment can be made from Edmund Optics(●), Thorlabs, Inc.(∗), Casix, Inc.(✠), U-oplaz Technologies(℩), CVI Laser LLC(‡), Pacer(◇), and National Instruments(†). Note that the SPCM power supplies are still unsettled.

3.2.3 Detection of Entangled Photons

The detector, Perkin-Elmer model SPCM-AQ4C, is an array of 4 Si Avalanche Photodiodes. Operated in Geiger mode, each channel detects single photons and gives a $25ns$ TTL pulse for output. The array can handle a maximum of count rate of 2Mc/s per channel and has a dark count rate of less than 500c/s. The module requires 2,5,and $30VDC$ power (see Table 3.1 for details). The SPCM-AQ4C IO module provides convenient connectors for power, gating functions(BNC), and detection signals(BNC) of the SPCM-AQ4C.

Coincidences are determined by a coincidence circuit, made with fast logic chips. The coincidence circuit for the Bell's inequality experiment has been built and tested. A slightly more complicated circuit will need to be built for experiments which utilise 3 or more detectors.

Counting is performed by a PCI counter/timer card on a personal computer. The PCI-6601 from National Instruments provides 4 counter/timers and can handle 20MHz data sources. The current coincidence circuit cannot produce faster than 4MHz data, which is well over the expected count rate. While this experiment uses only 3, other experiments may use all 4 counter/timers.

3.3 Additional Experiments

The apparatus for the Bell's inequality experiment can be extended to other experiments at a comparatively low cost[9]. In addition to those listed below, Colgate's website mentions a quantum eraser experiment[31]. The following schedule successively extends the original experiment.

Polarization states This experiment requires no additional equipment and will likely be performed as a same lab precursor to the Bell's inequality experiment. It involves varying the phase angle ϕ between the vertical and horizontal components of the pump light, which in turn varies the entangled state according to $|\psi_{DC}\rangle = 1/\sqrt{2}(HH + e^{i\phi}VV)$. Measurements are taken with fixed polarization filters while ϕ is adjusted. Students can work out the calculations for and confirm experimentally the quantum mechanics model which predicts the polarization states for ϕ, pump angle θ_l, and polarizer angles α and β.

The photon exists This is the experiment performed recently at Whitman College[10]. The main pieces of additional equipment total to $800.

$104 Broadband polarizing beamsplitter, (BPS0102) Casix

$67 Prism mount and holder, (KM100P) Thorlabs

$142 $810nm$ half wave plate, Casix

$80 Rotation Stage, (RP01) Thorlabs

$266 Collector Assembly

$140 Two fibers and FC-FC L-bracket sleeve

Single photon interference This experiment requires an interferometer to vary possible photon path lengths before recombination at a beam splitter. The interferometer which offers the most stability and easiest alignment seems to be the polarization interferometer[32]. The total cost of the following additional equipment is $1200.

$900 Two beam displacers, (BD27) Thorlabs

$142 $810nm$ half wave plate, Casix

$80 Rotation Stage, (RP01) Thorlabs

$75 Rotary Mount, (RSP1) Thorlabs

Biphoton interference Mirrors in kinematic mounts are needed for this experiment. I estimate an additional cost of $500.

3.4 Summary

The experiment presented in this chapter to test a Bell inequality is suitable for advanced undergraduates. The equipment provides a quality nonlinear optics platform on which to build other quantum optics experiments. While the initial investment of $19600 is high, additional experiments can be sequentially purchased for much less, about $1000 each. These experiments are being developed for undergraduate laboratory students at other institutions around the country. Funding these experiments at Oberlin will provide fresh inspiration in the lab classes and allow the possibility of cutting edge quantum optics research.

Chapter 4: Experiment

This chapter describes an experiment to test a Bell inequality with entangled photon polarization states. It covers the production and detection of entangled photons and procedures for alignment, system verification, and data collection. Fig. 3.1 shows a diagram of the experimental setup. The rate of coincident detection of photons between two photodetectors is the dependent variable in all cases. This rate is measured by setting a fixed time period T for data collection and measuring the number of coincidence detections N. The number of coincidences N is a function of the angle settings α and β of the linear polarizers.

4.1 Production of Entangled Photons

The pump laser produces more than $20mW$ of linearly polarized light at $405nm$ in a beam of diameter less than $1.5mm$. The spectral linewidth is less than $1nm$. The laser may take as many as 15 minutes to warm up, so it is best to keep it on during experimental sessions[33]. The module has a shutter which can block the beam when it is not in use. Take appropriate safety precautions: do not look into the laser beam; use the beam stop and laser shutter; eliminate stray reflections. Align the pump beam to be level with the optics table.

A quartz half wave plate (HWP) in a rotary mount is placed in the path of the laser beam to adjust the polarization angle of the laser light. Rotation of the HWP optic axis by θ relative to the polarization direction of the laser will result in a rotation by 2θ of the laser polarization angle[34]. The HWP is zero order, air-spaced, cut for $400nm$, and is AR coated[35]. It should be aligned to retroreflect the pump laser.

A quartz quarter wave plate (QWP) on a rotation stage is placed in the laser beam path after the HWP to adjust the phase ϕ between horizontally and vertically polarized components of the beam. The optical axis of the QWP should be in-line with the axis of the rotation stage. Tilting the QWP about the optic axis adjusts the phase ϕ between horizontally and vertically polarized components of the downconvtered light.

Non-linear crystals in the laser beam path after the QWP produce entangled photons by type-I spontaneous parametric down-conversion (see Section 2.2). The crystals are beta barium borate (BBO, $\beta\text{-}BaB_2O_4$), a highly non-linear birefringent material with low hygroscopic susceptibility, high damage threshold, and wide phase-matching ranges. Two identical BBO crystals are custom cut and mounted orthogonally so that degenerate daughter photons are entangled and emerge on opposite sides of the cone with opening angle approximately 3°. The BBO should be aligned to retroreflect the pump laser.

4.1.1 Expected Production Rate

In the power series expansion for the polarization of a material due to an electric field $\mathbf{E}$, the ratio of the quadratic term to the linear term can be found as follows:

$$\left|\mathbf{P}^{(1)}\right| = \epsilon_0 \chi^{(1)} \left|\mathbf{E}\right|$$
$$\left|\mathbf{P}^{(2)}\right| = \epsilon_0 \chi^{(2)} \left|\mathbf{E}\right|^2$$

$$\frac{P^{(2)}}{P^{(1)}} = \frac{\chi^{(2)}}{\chi^{(1)}} E_0.$$

The linear susceptibility is related to the index of refraction as $\chi^{(1)} = n^2 - 1$, and the quadratic susceptibility is $\chi^{(2)} = 2 \cdot d_{\text{eff}}$. The index of refraction for BBO is about 1.7 at $400nm$. For type-I down-conversion in BBO, $d_{\text{eff}} = d_{31} \sin\theta$, where $d_{31} = 0.15pm/V$ and θ is the angle between the electric field and the optic axis (90°-30° for our crystals). Our laser has a calculable intensity of about $10^4 W/m^2$, which implies a maximum electric field $E_0 \approx 3 \cdot 10^3 V/m$. Plugging it all in, we get

$$\frac{P^{(2)}}{P^{(1)}} \approx 10^{-10}$$

This is approximately the factor of attenuation we can expect from pump laser to down-converted photon pairs. A $20mW$, $405nm$ beam has about $4 \cdot 10^{16}$ photons per second, so we can expect to create about 10^6 down-converted pairs per second. However, not all of these will be degenerate pairs on the cone we observe. Furthermore, our detector lenses only cover a small arc length of this cone, about $2x8mm$ of a $200mm$ circumference circle, or 10%. After taking into account attenuation from linear polarizers (70% max transmission) and detectors (50% efficient), we can expect to detect no more than 5000 entangled pairs per second.

This result is consistent with reports on this method of entangled photon generation. Kwiat et. al. give 140 entangled pairs per second per mW of pump power as a rule of thumb[6]. This corresponds to $3000/s$ for our $20mW$ pump laser. Another group reported rates of 300 entangled pairs per second using a $5mW$ laser[8]. Our downconverted beam, with the $20mW$ pump, should be four times more efficient as well as four times more powerful, so we can expect $4^2 \cdot 300/s = 5000/s$.

4.2 Photon Collection and Detection

The entangled photons from degenerate downconversion pairs lie on a cone, the opening angle of which is determined by the crystal cut to be about 3°. Because the system has radial symmetry, alignment can be made easier by mounting the photon collection components on rails which pivot about the crystal mount. At the distance of the hinge plus optic rail combination from the source, about $1.3m$, 3° corresponds to $7cm$ from the centerline. It might be a good idea to put screws in the optic table to limit rail freedom to a small angular range.

On each rail are three components of the data collection equipment, an iris diaphragm, a near infrared linear polarizer in a rotary mount, and a collector assembly consisting of a bandpass interference filter and a fiber coupling lens in an adjustable mount. These three components should be mounted on each rail in the order above, moving away from the downconversion crystals. The bandpass filter can be unscrewed and removed from the collector assembly to allow reverse laser alignment, and also to allow swapping of filters should it become desirable in the future. The signal through these three components is attenuated. Closing the iris diaphragms purifies the entangled state detected[1], at the cost of signal attenuation. The linear polarizers transmit at most 70% of vertically polarized light. The bandpass filters have a minimum peak transmission of 50%.

After collection, light from the two assemblies is channelled via fiber optic cable to avalanche photodiodes which can detect single photons. The fibers are multi-mode with $62.5\mu m$ cores and standard FC type connections on both ends. Each fiber path from collector to photodiode should use two fiber cables coupled through a connector sleeve so that the laser alignment fiber can be easily be swapped in and out of each path.

The photodiodes can detect single photons with an efficiency of about 50% for light at $800nm$. They are often called single photon counting modules (SPCMs). The photodiodes are very sensitive and expensive, and so must be used with great caution. Section 4.2.1 describes necessary precautions. Each SPCM has a fiber (FC) connection aligned to its input, and a $25ns$ TTL pulse is emitted upon detection of a single photon. There are no external settings. A card edge connector module attaches to the SPCM-AQ4C to provide a power connection and BNC connections for gating functions (not used here) and output signals. To ensure proper operation, each BNC signal output connection must be grounded through a 50Ω load even if that module is not being actively used.

This experiment uses two of the four detector modules, and those outputs are connected via BNC cables to a coincidence detection circuit. The coincidence detector has a coincidence window of $25ns$, and emits $250ns$ TTL pulses at three output ports: one for each original signal and one for coincidence detections. See Chapter 6 for further details concerning the coincidence circuit. The $250ns$ TTL pulses from the coincidence circuit are easy to detect and count with a counter/timer data acquisition (DAQ) card in a personal computer.

4.2.1 Care of Avalanche Photodiodes

Avalanche photodiodes work by maintaining a high bias voltage across a piece of silicon, near the dielectric breakdown threshold. Photons with wavelength from visible to infrared can cause an electron-hole pair to form in the the silicon, like in a solar cell. The high voltage bias across the silicon in the avalanche photodiode causes the

---

[1] Photon pairs collected over a finite solid angle and wavelength range will have a spread in the phase lag ϕ. The actual state collected will involve $\langle \cos \phi \rangle = \cos \phi_m$. The state collected can be purified by closing the irises so that $\cos \phi_m \to \cos \phi$ for a single value of ϕ.

electron-hole pair to be separated and accelerated. Collisions cause more electron-hole pairs to be formed, and the cascading process results in detectable dielectric breakdown. The circuitry in the module stops the process before damaging the silicon, and allows the voltage to be stabilized (reset) quickly. The result is a very sensitive single photon counter.

The SPCM-AQ4C is an array of four avalanche photodiodes. Please read the manuals before operating this module[36, 37, 38], and observe the following precautions:

Overload Protection Each photon detection event generates heat in the detector, which is removed to a heatsink by a thermoelectric cooling circuit. This circuit can keep up with a maximum continuous count rate[2] of $2Mc/s$ per channel and a peak count rate of $5Mc/s$ per channel for intervals of $500ms$. At higher count rates the detectors will be damaged due to diode self-heating. To avoid detector overload, all fibers and connections leading to the SPCM should be completely light-tight, so that only light transmitted by the bandpass filter reaches the detector. Unused detector channels should be covered with FC termination caps. Finally, the detectors should only be operated in low-level lighting conditions, with only wavelengths far from the $810nm$ passband of the filter; blue or green LEDs satisfy the lighting requirements.

ESD Precautions The case of the SPCM-AQ4C has open sides to allow good ventilation. The open sides expose sensitive electronics, and sources of electrostatic discharge should be kept away from the detector.

High Voltage The module has internal sources of high voltage power. Take care to keep fingers and implements away from the board and components on the board when it is under power.

Ventilation The module is designed to operate at temperatures from 5°C to 40°C, and is thermoelectrically cooled through a heat sink. Unrestricted airflow over the heat sink is important for maintaining an appropriate operating temperature.

AM 1.5 radiation in the passband of the filter amounts to about 10^{15} photons per second incident on an area of $1cm^2$. Normal indoor lighting is many orders of magnitude less intense than AM 1.5, but still supplies several orders of magnitude more photons per second than the detectors can handle. A fluorescent lighting incident with the SPCM might not be as disastrous as one involving an incandescent light because fluorescent sources produce most of their radiation at sharp peaks between 500 and $650nm$[39]. Even so, it would be a good idea for the final realization of this experiment to employ an interlock on the SPCM power supply so that it shuts off under overload conditions. The interlock could be triggered by dependence on extinguished lights and shut doors, by a simple photometer, or by count rates from the coincidence circuit outputs.

---

[2] million counts per second.

4.3 Alignment Procedure

The alignment procedure described here is derived from the procedures described in [7, 8, 10]. To align the equipment, begin by following the alignment guidelines in the preceding sections.

Set the pump laser to be level with the optics table by using either a laser mount or two mirrors. The beam stop should be placed in the pump beam path about a meter away. Next set up the optics rail and hinge combinations to pivot about the BBO mount in a limited range, no wider than 5° from the centerline defined by the pump beam. The pivot range can be limited by putting screws in the optics table. Each optics rail should have an iris diaphragm, a linear polarizer, and a collector assembly (CA) mounted on it. Next, set the BBO on its post so that it retroreflects the pump laser. Mount the quarter wave plate between the pump and the BBO on a rotation stage so that it can be tilted about its optic axis. Initially, the the QWP should retroreflect the pump laser. Mount the half wave plate between the pump and the QWP in a rotary mount so that it also retroreflects the laser.

A HeNe laser coupled into a fiber cable can be used to help align the apparatus. Set the HeNe to be incident onto the fiber collimating lens, and adjust the lens with the kinematic mount so that light transmitted through to the other end seems maximal. Be careful not to look directly into the fiber.

From one collector arm remove the linear polarizer from its post holder, open the iris diaphragm completely, and unscrew the bandpass filter from the CA. Connect the HeNe laser's fiber at the mating sleeve so that it shines out of the CA. Set the CA kinematic mount to be square with the table (by moving it to an extreme) and use the coarse translational and angular adjustments on the CA post holder to make the HeNe beam overlap the pump beam on the BBO. Use the fine adjustments of the kinematic mount to adjust the CA so that the position of the HeNe beam remains stable in overlapping the pump beam throughout the angular range of the rail. Lock the kinematic mount. Narrow the iris diaphragm and adjust its position so that it is centered about the HeNe beam. Replace the bandpass filter on the CA, the linear polarizer in its post holder, open the iris, and swap the HeNe out of the fiber path to the SPCM. Repeat this process for the second arm. Turn off the HeNe laser and shutter the pump laser.

At this point the room can be prepared to operate the SPCM, and all electronics should be wired correctly. Double check the SPCM to make sure all four inputs are covered and all four outputs are 50Ω terminated.

When all is ready, turn on the photon counting array and make sure that it has a stable dark count. The dark count rate should be fewer than $500c/s$ for these SPCMs. Set the polarizers to the same angle, unshutter the pump laser, and monitor each detector's singles count rate and the coincidence count rate. Adjust the rails about their pivots to maximize the coincidence rate, and then clamp them in place. It may help to maximize the coincidence rate to first try to maximize the singles rate in each detector. The maximum coincidence rate should be several thousand coincidence counts per second. If desired, the fine settings of the CA kinematic mounts can be perturbed in search of the maximum coincidence rate after the rails are clamped.

4.4 Testing of Polarization States

After the optics are aligned, the polarization state of the downconverted pairs can be optimized and tested by adjusting the pump variables θ_p and ϕ_p. First, equalize the coincidence counts for polarizer settings $(0,0)$ and $(\frac{\pi}{2}, \frac{\pi}{2})$ by rotating the half wave plate to adjust the pump angle θ_p. Equal coincidence rates along any two orthogonal polarization vectors imply that θ_p is at an angle of $\pi/4$ relative to the two orthogonal downconversion crystals. The phase difference $\phi = \phi_p + \Delta$ between horizontally and vertically polarized components of the downconverted light varies monotonically with the QWP tilt angle δ.

Verify that you can control the state $|\psi\rangle$ of downconverted pairs by setting the linear polarizers to $(\frac{\pi}{4}, \frac{\pi}{4})$ and varying δ so that ϕ goes through several multiples of 2π. The best fit curve through these data points will be a maximum for ϕ an even multiple of π, corresponding to the state $|\psi_{DC}^+\rangle$, and a minimum for ϕ an odd multiple of π, corresponding to the state $|\psi_{DC}^-\rangle$, where $\psi\pm = HH \pm VV$ is the state predicted by Eq. 2.19. This verification could also be done with the linear polarizers set to $(\frac{\pi}{4}, \frac{3\pi}{4})$, so that maximums correspond to $|\psi_{DC}^-\rangle$ and minimums correspond to $|\psi_{DC}^+\rangle$.

4.5 Data Collection

The data collection procedure described here gives methods for calibrating the equipment and collecting data which violates the Bell inequality described in Section 2.1. The first set of data should be taken with irises completely open. Subsequent data sets may purify the entangled state collected by utilizing smaller aperture irises, as described by footnote 1. In the following text, coincidence rate will be referred to by the number of counts $N = N(\alpha, \beta)$ in a fixed time period T for linear polarizer angles set to α and β respectively. T will hereafter be dropped from references to the coincidence rate.

Set the state to $|\psi_{DC}^+\rangle$ and calibrate the equipment by finding the experimental dark coincidence count rate C and the rate of entangled photon production A. C is the coincidence rate with the linear polarized set to orthogonal angles. For example,

$$C = N(0, \pi/2). \tag{4.1}$$

The entangled photon production rate A is the sum of two orthogonal measurements of parallel linear polarizers, minus twice C. For example,

$$A = N(0,0) + N\left(\frac{\pi}{2}, \frac{\pi}{2}\right) - 2C. \tag{4.2}$$

Also measuring $N(\frac{\pi}{4}, \frac{\pi}{4})$ will allow an estimate of the purity of the entangled state (see section 5.1).

The quantity S of the CHSH Bell inequality is a function of four angles (a, a', b, b'). $|S| \leq 2$ for any local hidden variable theory. For the state $|\psi_{DC}^+\rangle$, quantum mechanics predicts a maximum $S = 2\sqrt{2}$ at the angles $(-\frac{\pi}{4}, 0, -\frac{\pi}{8}, \frac{\pi}{8})$. See Chapter 2 and Eq. 2.10, 2.20, and 2.26. To find S experimentally, measurements of N must be taken

α	β	N_A	N_B	N
-2	-1			
-2	1			
-2	3			
-2	5			
0	-1			
0	1			
0	3			
0	5			
2	-1			
2	1			
2	3			
2	5			
4	-1			
4	1			
4	3			
4	5			

Table 4.1: Detector settings for collection of N_A, N_B, and N such that $S > 2$. The detector settings α and β are given in units of $\pi/8$ radians, or 22.5°.

at sixteen detector settings. In addition to recording the coincidence rate N, record the singles rate in each detector, N_A and N_B. The detector settings of necessary measurements for $S(-\frac{\pi}{4}, 0, -\frac{\pi}{8}, \frac{\pi}{8})$ are given in Table 4.1.

After these data are taken, it may be interesting to repeat the experiment with greater purity of the entangled state by reducing the iris size. Additionally, one could set the state to $\left|\psi_{DC}^-\right\rangle$ and take data with some other appropriate set of 4 angles to show this state also violates $|S| \leq 2$.

Chapter 5: Analysis

This chapter describes how to analyze the collected data to determine the purity of the entangled state and to show a violation of the CHSH Bell inequality, that $|S| \leq 2$. One thing to notice when analyzing data from this experiment is whether or not it would be better fit to the model if all the settings of the polarizer angle α (β) where slightly different, as it is somewhat likely that the polarizer is mislabled by a few degrees. Another thing to think about is the rate of accidental coincidences of photons which are not entangled. This should be about $N_{ac} = \tau N_A N_B / T$, where τ is the coincidence window, N_A, N_B are the singles counts in each detector, and T is the time period of collection. Accidental counts can be shown to decrease S in the same way that C decreases S, as shown in Section 5.2 below.

5.1 Purity of Entanglement

Photon pairs collected over a finite solid angle and wavelength range will have a spread in the phase lag ϕ. The actual state collected will involve $\langle \cos \phi \rangle = \cos \phi_m$. The purity of the entangled state detected for $|\psi^{\pm}\rangle$ can be characterized by ϕ_m. For pure states of $|\psi^{\pm}\rangle$, $|\cos \phi| = 1$. Since 1 is the maximum, a distribution of ϕ will have $|\langle \cos \phi \rangle| < 1$. The closer $|\cos \phi_m|$ is to 1, the purer the entangled state detected.

A rough estimate of $\cos \phi_m$ can be found for $|\psi_{DC}^{+}\rangle$ using $N(0,0)$, $N(\frac{\pi}{2}, \frac{\pi}{2})$, $N(\frac{\pi}{4}, \frac{\pi}{4})$, and $N(0, \frac{\pi}{2})$ as follows. From Eq. 4.1 and 4.2 we know the dark rate of coincidence C and the total number of entangled pairs produced A. The number collected in time T for polarizer angles α, β should be the total production rate A times the probability $P_{VV}(\alpha, \beta)$ that any given pair both pass the polarizers, plus the dark rate C[1]. Then we have

$$N(\alpha, \beta) = A \cdot P_{VV}(\alpha, \beta) + C, \tag{5.1}$$

where P_{VV} is given by 2.24. A little arithmetic manipulation of this equation shows that

$$\frac{N(0,0) - C}{N(\frac{\pi}{2}, \frac{\pi}{2}) - C} = \tan^2 \theta, \tag{5.2}$$

and

$$\frac{1}{\sin 2\theta} \left(4 \frac{N(\frac{\pi}{4}, \frac{\pi}{4}) - C}{A} - 1 \right) = \cos \phi_m. \tag{5.3}$$

Note that the four measurements needed for this type of calculation are different when the state is $|\psi_{DC}^{-}\rangle$ because $N(0,0)$ and $N(\pi/2, \pi/2)$ are both approximately C, and Eq. 4.1 will not be C. Given a more extensive data set, the values C, A, θ, and ϕ_m can be determined by the best fit of Eq. 5.1.

---

[1] For simplicity, the accidental count rate is ignored. It acts to increase C

5.2 Bell Inequality Violation

Remember from Eq. 2.10 that

$$S = E(a, b) - E(a, b') + E(a', b) + E(a', b')$$

for any four angles (a, a', b, b'). The expression $E(\alpha, \beta)$ from Eq. 2.20 requires four measurements, so $S(a, a', b, b')$ requires sixteen in general. In order to find S from the data we need find an expression relating it to N. Using Eq. 2.20 and 5.1, one can show

$$\frac{N(\alpha, \beta) + N(\alpha \perp, \beta \perp) - N(\alpha, \beta \perp) - N(\alpha \perp, \beta)}{N(\alpha, \beta) + N(\alpha \perp, \beta \perp) + N(\alpha, \beta \perp) + N(\alpha \perp, \beta)} = \left[\frac{1}{1 + 4\frac{C}{A}} \right] E(\alpha, \beta). \quad (5.4)$$

Because C and A are positive, the multiplier of E in the above equation can only decrease the value, which can only decrease $|S|$. Since we are interested in violating $|S| \le 2$, and $C \ll A$ anyway, we can ignore the multiplier and use the left hand side as an expression for E, and so find S.

The uncertainty[40] in a counting data set is

$$\sigma_n = \sqrt{n}, \quad (5.5)$$

and the uncertainty in a function $q = q(x, \ldots, z)$ is

$$\sigma_q = \sqrt{\left(\sigma_x \frac{\partial q}{\partial x} \right)^2 + \ldots + \left(\sigma_z \frac{\partial q}{\partial z} \right)^2}, \quad (5.6)$$

where $\partial q / \partial x$ is the partial derivative of q with respect to x. This implies that the uncertainty in S is

$$\sigma_S = \sqrt{\sum_{i=1}^{16} \left(\sigma_{N_i} \frac{\partial S}{\partial N_i} \right)^2}.$$

In light of Eq. 5.5 we can substitute $\sqrt{N_i}$ for σ_{N_i} and get

$$\sigma_S = \sqrt{\sum_{i=1}^{16} N_i \left(\frac{\partial S}{\partial N_i} \right)^2}. \quad (5.7)$$

In general this expression for the uncertainty is complicated, and is easiest evaluated by a computer.

If upon analyzing the data we find $|S| \le 2$ no conclusion can be drawn about the validity of a local hidden variable theory. However, if we find $S > 2$, as predicted by quantum mechanics for some settings, the data shows a violation of the CHSH Bell inequality derived in Section 2.1.2. Thus the data cannot be described by any local hidden variable theory.

The interpretation of non-locality or alocality in nature is more a matter of philosophy than of physics. Alocality does not pose problems for special relativity. Although the measurement of one particle results in a superluminal influence on the other particle, that influence carries no energy and, since the result of either measurement seems random without knowledge of the other, no information. David Griffiths asks us to consider the distant shadow of a ladybug as it walks across a projector lens illuminating a distant screen[16]. At far enough distances of the screen, the leading edge of the ladybug's shadow propagates faster than the speed of light. Perhaps the difficulty in accepting alocality stems from failing to recognize the shadow of a larger system.

Chapter 6: Coincidence Detection Electronics

Experiments in quantum optics utilizing entangled photons rely on the coincident detection of two or more photons. Some experiments of this type use combinations of time-to-amplitude converters (TAC) and single-channel analyzers (SCA) to detect coincident signals from the photodetectors[5, 6, 10]. The TAC/SCA combinations cost several thousand dollars. This chapter describes a fast logic circuit which fulfils the coincidence counting requirements and can be built for under $40. The circuit is designed to receive $25ns$ TTL signals and detect coincidences in a $25ns$ window. The output signals are designed to be $250ns$ TTL pulses. The coincidence window is not adjustable, but a similar circuit with a different coincidence window is easy to design. Additionally, the design of this circuit can be extended to detect pairs of coincidences between more than two inputs.

A circuit was built according to this design and tests showed it had a coincidence window of between $18ns$ and $30ns$. The output signals where clear and should be easy to count, with a digital counting card for example. The following sections document the design, construction, and performance of the coincidence circuit.

6.1 Design

The design for this circuit was published in 2002 by Dehlinger and Mitchell[7]. The only changes from their design to the one described here are two capacitors added for power stability[41]. A schematic is shown in Fig. 6.1(a). The circuit consists of two 74ACT74 dual D-type positive edge-triggered flip-flops, or 4 flip-flops total. Input pulses terminate into a 50Ω load as required by the photodetectors.

Chips 1 and 4 simply relay a pulse received on K to $\overline{Q}$. The duration of the pulse from $\overline{Q}$ depends on the time constant of the RC combination between Q and $\overline{S}$, which for the resistor and capacitor chosen is $1k\Omega \cdot 220pF = 220ns$. This pulse duration should be easy to count with a computer data acquisition card.

Chip 3 in the circuit delays the signal at B_{in} for the time needed to clock and reset, typically $13ns$, with a minimum of $6.5ns$ and maximum of $19.5ns$[42]. In the case of coincident input, the signal from A_{in} sets D on chip 2 to HIGH before the rising pulse from the delayed B_{in} triggers the circuit. From the truth table (Table 6.1) it is clear that this combination will issue HIGH on Q, the coincidence output. The RC reset on chip 2 determines the length of the coincidence signal as in chips 1 and 4. Coincidence detection can only occur while A_{in} is HIGH, so the coincidence window for the $25ns$ input pulses is $25ns$.

| Inputs				Outputs	
$\overline{S}_D$	$\overline{C}_D$	K	D	Q	$\overline{Q}$
L	H	x	x	H	L
H	L	x	x	L	H
L	L	x	x	H	H
H	H	$\_\Gamma$	H	H	L
H	H	$\_\Gamma$	L	L	H
H	H	L	x	Q_0	$\overline{Q}_0$

Table 6.1: The truth table for each half of a 74ACT74 logic chip. H, L, $\_\Gamma$, and x correspond to TTL HIGH, LOW, rising, and immaterial voltages, respectively[42].
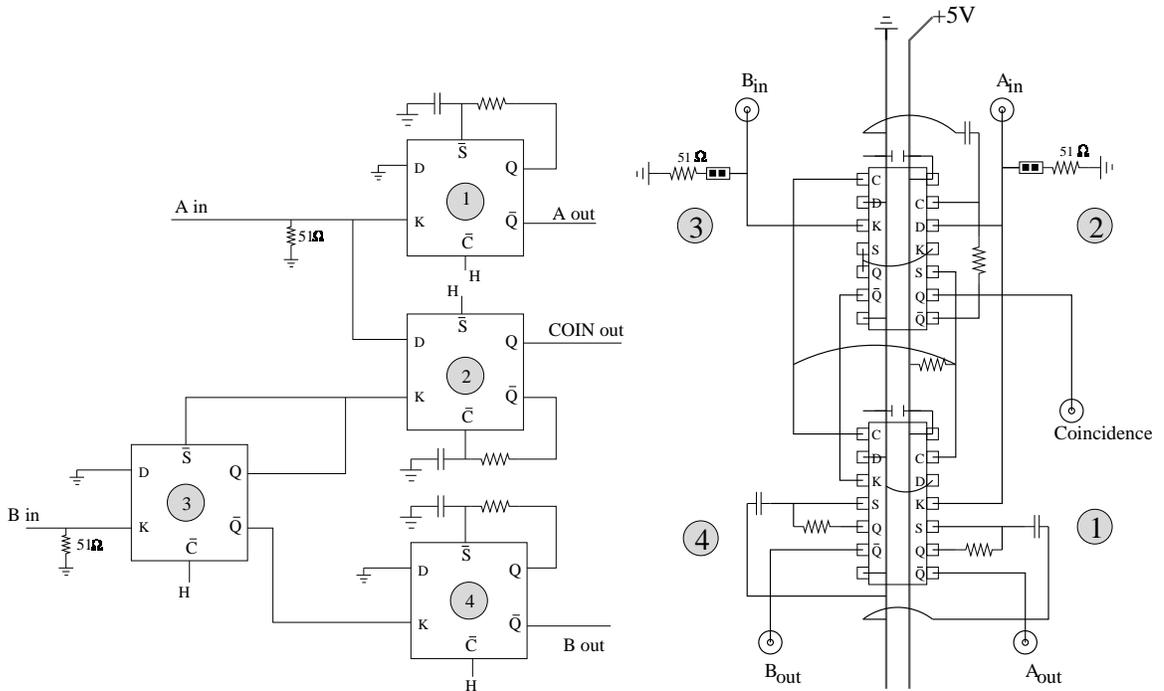
(a) A schematic diagram of the coincidence detection circuit. Each square is half a 74ACT74 logic chip. H indicates TTL high, $+5V$.

(b) Diagram of the circuit layout as constructed, including jumpers and additional capacitors across the bus.

Figure 6.1: Two schematic diagrams of the coincidence detection circuit. All capacitors are 220pF except the two across the bus. All resistors are 1kΩ except the two labeled 51Ω.

41
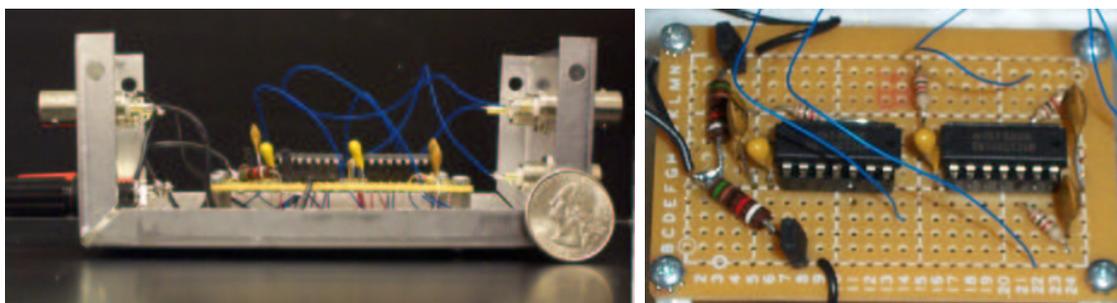
(a) Side view.	(b) Close up.

Figure 6.2: Pictures of the coincidence circuit.

6.2 Construction

The layout of the circuit is shown in Fig. 6.1(b) as assembled on a perforated circuit board with components on top and solder and wiring underneath. Each hole of the board is surrounded by a copper pad to which solder adheres easily. All components are listed in Table 6.2.

The central bus provides stable power and ground to the whole circuit. It was made by soldering two segments of 22 gauge wire to each pad in adjacent rows. By only stripping the portion of the wire to be soldered the wire on the top side remained covered.

The two 14 pin sockets were placed to straddle the bus, and were soldered at each pad. The sockets allow for easy replacement of the logic chips, should it be necessary. A $22\mu F$ capacitor was placed across the bus next to the power pin of each chip to increase power stability. A 1kΩ was placed between the bus and the connection point for TTL HIGH for chip protection.

Twenty-two gauge wire was chosen for A_{in} and B_{in}, but that choice was unimportant. All remaining wires are 30 gauge because the interconnection soldering is tight and would be difficult to manage with large wire. The wires for the output signals were threaded back up through the board so that any strain is put on the sheathed portion of the wire instead of the connections.

The 51Ω terminations on the inputs are the necessary load required by the photodetectors, but are inhibitory during testing of the circuit. They were joined to the inputs through jumpers so that the terminations can be disconnected by removing the jumper caps.

The completed circuit is mounted inside a metal box to provide electromagnetic shielding and mounts for BNC and banana jacks. The input and output signals travel on BNC cables and the power comes through banana jacks. The connecter holes were drilled with a drill press and drill bit sizes $\frac{25}{64}$ and $\frac{5}{16}$ for the BNC and banana jacks, respectively. It was easy to solder wires into the BNC jacks. However, solder did not bond well to the banana jack posts or to the box. In order to avoid the

Item	Qt.	$/item
51Ω resistor	2	< 1
1kΩ resistor	4	< 1
$220pF$ capacitor	3	< 1
$22\mu F$ @$16V$dc capacitor	2	< 1
14-pin socket	2	< 1
74ACT74 logic chip	2	< 1
Jumper pins	2	< 1
Project box	1	3
Perforated circuit board	1	2
Banana jack panel mount	2	1
BNC panel mount	5	1
22 gauge solid wire		
30 gauge solid wire		
Total		< 40

Table 6.2: Materials used to build the coincidence circuit.

need to solder the bus ground to both a banana post and the box, it would be better to use a special grounding banana jack. Fig. 6.2 shows pictures of the completed circuit.

The following are useful notes for anyone attempting to create a similar circuit.

- It is difficult to strip 30 gauge wire without a wire stripper.

- The stripped portions of any gauge wire are much weaker than the protected portions. The sheath should be kept wherever possible and stripped portions should be bent as little as possible to avoid breaking.

- The 30 gauge wire is easier to solder and more robust if it is inserted into the perf board hole than if it is laid sideways on the board.

- Some of the connections between pins of the socket and the bus can be made without wire, just by connecting the blobs of solder.

- Although some of the components in this circuit were not trimmed short enough to rest on the board, such trimming is a good idea in general since it prevents possible undue strain on the copper pads underneath.

- A special grounding banana jack (instead of insulated) is recommended for the ground connection, to remove the need to solder to both the banana post and the box.

6.3 Performance

The circuit was tested with a HP 8111A 20MHz function generator and an oscilloscope. The function generator can supply a signal which mimics the 25ns TTL signal from a photodetector we expect as input. The function generator is built for 50Ω signal termination. The oscilloscope was able to display the signals on the circuit inputs and outputs, but ringing made it necessary to use a scope probe, with its shielding connected to the circuit's ground.

  When the signal from the function generator was connected to A_{in}, A_{out} showed a 250ns pulse, while B_{out} and Coin$_{out}$ remained flat. Connecting the signal to B_{in} produced a 250ns pulse at B_{out}, while A_{out} and Coin$_{out}$ remained flat. When the function generator signal was connected to A_{in} and B_{in} at the same time it was necessary to disconnect a 50Ω termination by removing a jumper, so that the 50Ω load on the function generated was maintained. In this situation, with signal input at both A_{in} and B_{in}, all three outputs showed 250ns pulses.

  To make sure that sufficiently separated signals on A_{in} and B_{in} are resolved as not coincident, part of the signal from the function generator was subjected to the propagation delay of a 7408 2-input positive AND gate. The propagation delay for that chip is typically 9ns according to the datasheet. When one input received the signal from the function generator and the other input received the signal delayed through 2 AND gates, there was no coincidence detected. However a delay of 1 AND gate was not enough to prevent coincidence detection. This is direct evidence that the circuit has a coincidence window of between 18ns (signal 9ns away on either side are coincident) and 36ns (signal 18ns away on either side are not). This fits our expectation that the window is 25ns, the length of the signal at A_{in}.

6.4 Summary

The circuit described in this chapter detects coincidences for 25ns 50Ω terminated TTL pulses with a coincidence window of 18ns to 36ns. This is ideal for quantum optics experiments which rely on coincident detection of photons using photodetectors such as the SPCM from Perkin-Elmer. The circuit can be constructed easily and for less than $40, and can be tested using a function generator and oscilloscope. As an end note, this circuit can be easily extended to accommodate three or more input signals, as shown in Fig. 6.3. Quantum optics experiments with a gating detector and two signal detectors are common and would use this extended circuit.
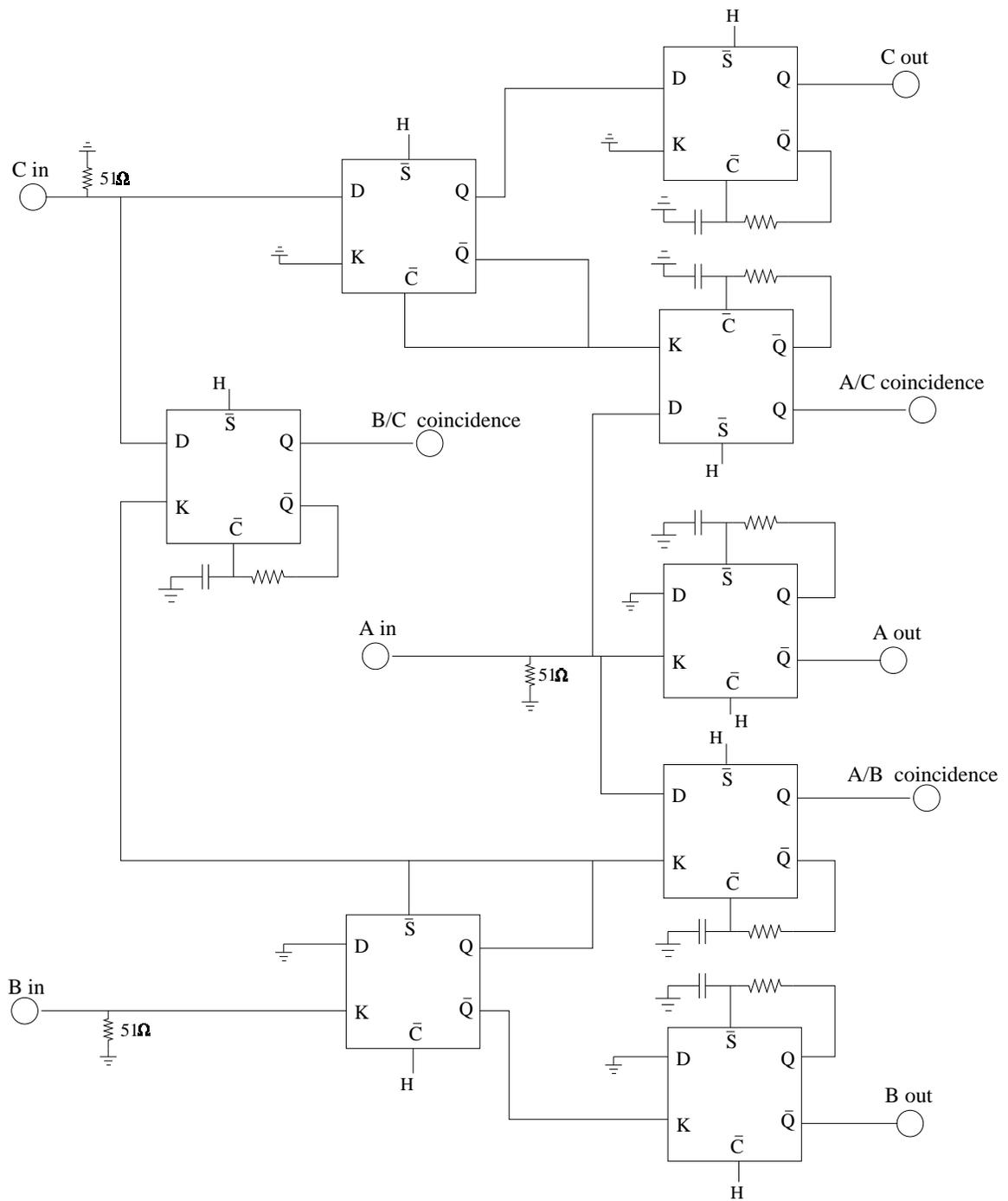
Figure 6.3: The coincidence circuit extended to detect coincidences between pairs of any three inputs.

Chapter 7: Summary

Undergraduate quantum optics experiments have become possible in the past few years due to advances in optical techniques and technology. Several colleges have now developed such experiments, and Oberlin College is poised to develop a Bell's inequality experiment of its own. This thesis is an accumulation point of all the work done so far on the project, and as such will be an important resource for those continuing the development.

The most important result of the project presented here is the finalized proposal for the experiment and equipment. The total equipment cost is $19600, with the most expensive pieces of equipment being the $9000 photodiode array and the $5000 $405nm$ pump laser. In addition to enabling a Bell inequality experiment, the equipment establishes a base for a series of quantum optics experiments accessible to undergraduates. The equipment may be used eventually for original research.

The thesis contains several other major chapters, dealing with the theory of major components, descriptions of experimental methods, outlines of data analysis, and the design and construction of the coincidence detecting electronics. The theory chapter provides relevant details for anyone trying to gain an understanding of the experiment. It covers Bell inequalities, nonlinear optics, the production of entangled photons via parametric downconversion, and quantum derivations for polarization state probabilities. The chapter on experimental methods provides the basic material for a laboratory manual. The chapter concerning the coincidence circuit will be important reading for anyone trying to build an extended coincidence circuit for a related experiment.

The Bell inequality experiment will be an exciting addition to the Advanced Lab rotation. With proper care and use, Oberlin will have excellent quantum optics equipment for years to come.

References

[1] A. Einstein, B. Podolsky, and N. Rosen. Can quantum-mechanical description of physical reality be considered complete? *Phys. Rev.*, 47:777–780, 1935.

[2] John S. Bell. On the einstein podalsky rosen paradox. *Physics*, 1(3):195–200, 1964. This article reprinted in [19].

[3] A. Aspect, P. Grangier, and G. Roger. Experimental tests of realistic local theories via bell's theorem. *Phys. Rev. Lett.*, 1981.

[4] A. Aspect, P. Grangier, and G. Roger. Experimental realization of einstein-podalsky-rosen-bohm gedankenexperiment: A new violation of bell's inequalities. *Phys. Rev. Lett.*, 49:91, 1982.

[5] Paul G. Kwiat, Klaus Mattle, Harald Weinfurter, and Anlon Zeilinger. New high-intensity source of polarization-entangled photon pairs. *Physical Review Letters*, 75(24):4337–4342, December 1995.

[6] Paul G. Kwiat, Edo Waks, Andrew G. White, Ian Appelbaum, and Philipe H. Eberhard. Ultrabright source of polarization-entangled photons. *Physical Review A*, 60(2):R773–R776, August 1999.

[7] D. Dehlinger and M. W Mitchell. Entangled photon apparatus for the undergraduate laboratory. *Am. J. Phys.*, 70:898–902, 2002.

[8] D. Dehlinger and M. W Mitchell. Entangled photons, nonlocality, and bell inequalities in the undergraduate laboratory. *Am. J. Phys.*, 70(9):903–910, September 2002.

[9] C. H. Holbrow, E. Galvez, and M. E. Parks. Photon quantum mechanics and beam splitters. *Am. J. Phys.*, 70(3):260–265, March 2002.

[10] J. J. Thorn, M. S. Neel, V. W. Donato, G. S. Bergreen, R. E. Davies, and M. Beck. Observing the quantum behavior of light in an undergraduate laboratory. *Am. J. Phys.*, 2004. Preprint.

[11] A. K. Ekert. Quantum cryptography based on bell's theorem. *Phys. Rev. Lett.*, 67:661–663, 1991.

[12] C. H. Bennett. Quantum cryptography using any two nonorthogonal states. *Phys. Rev. Lett.*, 1992.

[13] Gilles Brassard. A bibliography of quantum cryptography. http://www.cs.mcgill.ca/ crepeau/CRYPTO/Biblio-QC.html, 1998.

[14] Michael A. Neilsen and Isaac L. Chuang. *Quantum computation and quantum information*. Cambridge U. Press, 2000.

[15] Peter W. Shor. Polynomial-time algorithms for prime factorization and discrete logarithms on a quantum computer. *SIAM J. Comput.*, 26(5):1484–1509, 1997.

[16] David J. Griffiths. *Introduction to Quantum Mechanics*. Prentice Hall, NJ, 1995.

[17] N David Mermin. Is the moon there when nobody looks? reality and the quantum theory. *Physics Today*, April 1985.

[18] David Bohm. *Quantum Theory*. Prentice-Hall, Englewood Cliffs, NJ, 1951. pp. 614-619.

[19] M. Bell, K. Gottfried, and M. Veltman, editors. *John S. Bell on The Foundations of Quantun Mechanics*. World Scientific, NJ, 2001.

[20] J.F. Clauser, M.A. Horne, A. Shimony, and R.A. Holt. Proposed experiment to test local hidden-variable theories. *Phys. Rev. Lett.*, 23(15):880–884, 1969.

[21] Paul G. Kwiat, Philippe H. Eberhard, Aephraim M. Steinberg, and Raymond Y. Chiao. Proposal for a loophole-free bell inequality experiment. *Phys. Rev. A*, 49(5):3209–3221, May 1994.

[22] P. H. Eberhard. *Phys. Rev. A*, 1993.

[23] P. Grangier, G. Roger, and A. Aspect. Experimental evidence for a photon anti-correlation effect on a beam splitter: A new light on single-photon interferences. *Europhys. Lett.*, 1986.

[24] Robert W. Boyd. *Nonlinear Optics*. Academic Press, second edition, 2003.

[25] Xinping Zhang. *High-repitition-rate Femtosecond Optical Parametric Oscillators Based on KTP and PPLN*. PhD thesis, Philipps-Universität Marburg, Marburg, Germany, 2002. Chapter 2.

[26] Cleveland Crystals Inc. BBO and LBO. http://www.clevelandcrystals.com/BBOLBO.shtml.

[27] Almaz Optics Inc. BBO crystal. http://www.almazoptics.com/Bbo.htm.

[28] SDLN Coretech Crystal Co. Beta barium borate. http://www.coretech.com.cn/BBO.HTM.

[29] Paul G. Kwiat. *J. Mod. Opt.*, 44:2173, 1997.

[30] R. Y. Chiao, P. G. Kwiat, and A. M. Steinberg. Optical tests of quantum mechanics. In *Advances in Atomic, Molecular, and Optical Physics*, volume 34, pages 35–83. Academic, 1994.

[31] Photon quantum mechanics. Internet. `http://departments.colgate.edu/physics/research/Photon/photon_quantum_m%echanics.htm`.

[32] M.K. Beck. Modern quantum mechanics experiments for undergraduates. Internet, 2004. `http://marcus.whitman.edu/~beckmk/QM/`.

[33] Edmund Optics. Solid state lasers. `http://www.edmundoptics.com/`, April 2004.

[34] Eugene Hecht. *Optics*. Pearson Addison Wesley, 4th edition, 2001.

[35] Casix Inc. Waveplates. `http://casix.com/product/Waveplate.htm`.

[36] Perkin-Elmer Optoelectronics. Single photon counting module, SPCM-AQR series. Internet. Datasheet.

[37] Perkin-Elmer Optoelectronics. SPCM-AQ4C, single photon counting array. Internet. Datasheet.

[38] Perkin-Elmer Optoelectronics. *SPCM AQ4C Four Channel Photon Counting Module–User Guide*, May 2003.

[39] D.W. Finn and M. J. Ouellette. Compact fluorescent lamps: What you should know. *Progressive Architecture*, pages 89–92, August 1992.

[40] John R. Taylor. *Introduction to Error Analysis*. University Science Books, CA, second edition, 1997.

[41] William Mohler. Personal Communication, 2003. Oberlin College.

[42] Semiconductor Components Industries, LLC. *74ACT74 Datasheet*, May 2001. `<http://onsemi.com>`.